Oimatsu Satoshi (Orcid ID: 0000-0002-6757-6886)
Nosé Masahito (Orcid ID: 0000-0002-2789-3588)
Teramoto Mariko (Orcid ID: 0000-0001-5983-1149)
Yamamoto Kazuhiro (Orcid ID: 0000-0002-2515-8643)
Matsuoka Ayako (Orcid ID: 0000-0001-5777-9711)
Kasahara Satoshi (Orcid ID: 0000-0002-3479-772X)
Keika Kunihiro (Orcid ID: 0000-0003-0265-4318)
Le Guan (Orcid ID: 0000-0002-9504-5214)
Fujimoto Akiko (Orcid ID: 0000-0001-9686-6228)
Sormakov Dmitriy (Orcid ID: 0000-0003-2829-5982)
Tanaka Yoshimasa, -M. (Orcid ID: 0000-0001-7276-4868)
Shinohara Manabu (Orcid ID: 0000-0002-8931-9434)
Shinohara Iku (Orcid ID: 0000-0003-2700-0353)
Miyoshi Yoshizumi (Orcid ID: 0000-0001-7998-1240)
Slavin James, A. (Orcid ID: 0000-0002-9206-724X)
Ergun Robert, E (Orcid ID: 0000-0002-3096-8579)
Lindqvist Per-Arne (Orcid ID: 0000-0001-5617-9765)

Drift-bounce resonance between Pc5 pulsations and ions at multiple energies in the nightside magnetosphere: Arase and MMS observations

Oimatsu, S.[1], M. Nosé[1], M. Teramoto[2], K. Yamamoto[1], A. Matsuoka[3], S. Kasahara[4], S. Yokota[5], K. Keika[4], G. Le[6], R. Nomura[7], A. Fujimoto[8], D. Sormakov[9], O. Troshichev[9], Y.-M. Tanaka[10], M. Shinohara[11], I. Shinohara[3], Y. Miyoshi[2], J. A. Slavin[12], R. E. Ergun[13], and P.-A. Lindqvist[14]

[1] Graduate School of Science, Kyoto University

[2] Institute for Space-Earth Environmental Research, Nagoya University

[3] Institute of Space and Astronautical Science, Japan Aerospace Exploration Agency

[4] Graduate School of Science, University of Tokyo

This is the author manuscript accepted for publication and has undergone full peer review but has not been through the copyediting, typesetting, pagination and proofreading process, which may lead to differences between this version and the Version of Record. Please cite this article as doi: 10.1029/2018GL078961

[5] Graduate School of Science, Osaka University

[6] Heliophysics Science Division, NASA Goddard Space Flight Center

[7] Environmental Test Technology Unit, Japan Aerospace Exploration Agency

[8] International Center for Space Weather Science and Education, Kyusyu University

[9] Arctic and Antarctic Research Institute

[10] National Institute of Polar Research

[11] National Institute of Technology, Kagoshima College

[12] Department of Climate and Space Sciences & Engineering, University of Michigan

[13] Department of Astrophysical and Planetary Sciences, University of Colorado

[14]Royal Institute of Technology, Stockholm, Sweden

Key Points:

- A large-amplitude Pc5 wave is observed by Arase and MMS1 in the postmidnight region at $L > 5.4$ during the storm recovery phase.
- We estimate the *m*-number of the Pc5 wave to be −8 to −15 by using two independent methods with satellites and ground observations.
- We simultaneously observe the drift resonance for H^+ and O^+ ions at $\geq$ 56.3 keV and bounce resonance for O^+ ions at $\leq$ 18.6 keV.

Abstract

A Pc5 wave is observed by the Exploration of energization and Radiation in Geospace "Arase" satellite in the inner magnetosphere (L ~ 5.4–6.1) near postmidnight (MLT ~ 1.8–2.5 h) during the storm recovery phase on 27 March 2017. Its azimuthal wave number (m-number) is estimated using two independent methods with satellites and ground observations to be −8 to −15. The direct measurement of the m-number enables us to calculate the resonance energy. The flux oscillations of H^+ and O^+ ions at ≥ 56.3 keV are caused by drift resonance and those of O^+ ions at ≤ 18.6 keV by bounce resonance. Resonances of O^+ ions at multiple energies are simultaneously observed for the first time. The enhancement of the O^+/H^+ flux ratio at ≤ 18.6 keV indicates selective acceleration of O^+ ions through bounce resonance.

Plain language summary

Geomagnetic pulsations are magnetic fluctuations excited by solar wind or plasma instabilities in the magnetosphere. Pc5 waves are continuous geomagnetic pulsations with a period of 150–600 s. A Pc5 wave was observed in the inner magnetosphere during a magnetic storm on 27 March 2017. It propagated westward with a wave number of 8 to 15 and resonated with charged particles, resulting in oscillations of the H^+ and O^+ ion fluxes at ≥ 56.3 keV and the O^+ ion fluxes at ≤ 18.6 keV. Resonances of O^+ ions at multiple energies

are simultaneously observed for the first time. At the same time, the O^+/H^+ flux ratio at ≤ 18.6 keV enhanced corresponding to the O^+ ion flux oscillations, which indicates selective acceleration of O^+ ions through resonances.

1. Introduction

Dynamics of O^+ ions in the inner magnetosphere plays an important role for the ring current development and decay. Researchers have suggested that O^+ ions can be accelerated or decelerated through a wave-particle interaction with ultra-low frequency (ULF) waves called drift-bounce resonance (e.g., *Li et al.*, 1993; *Yang et al*., 2011a; *Keika et al*., 2013). The drift-bounce resonance condition is expressed as

$$\omega - m\omega_d = N\omega_b, \quad (1)$$

where ω is the wave angular frequency, ω_d is the particle bounce-averaged drift angular frequency, ω_b is the particle bounce angular frequency, and N is an integer (*Southwood et al.*, 1969). The drift-bounce resonance condition can be satisfied with odd mode waves when $N = 2k$ (where k is an integer), while it can be satisfied with even mode waves when $N = 2k+1$ (*Southwood and Kivelson*, 1982). Particles are accelerated or decelerated by oscillating wave electric field in the azimuthal direction of poloidal ULF waves (e.g., *Elkington et al*., 2003).

Azimuthal wave number (m-number) of ULF waves is an important parameter for the drift-bounce resonance because the resonance mode and energy are strongly dependent on it. ULF waves excited by internal instabilities tend to have a dominant magnetic oscillation in the radial direction and large m-number ($|m| > \sim 50$), while ULF waves excited by external sources tend to have a dominant magnetic oscillation in the azimuthal direction

and small *m*-number ($|m| < \sim 20$). To estimate the *m*-number, several methods have been proposed: phase delay method using multiple satellites (e.g., *Takahashi et al*., 1985, 2018; *Le et al*., 2017) or ground stations (e.g., *Baker et al*., 2003), and the finite Larmor radius effect method (e.g., *Min et al*., 2017; *Takahashi et al*., 2018).

To our knowledge, in these two decades, there have been only six observational studies about the drift-bounce resonance of O^+ ions at < 40 keV in which data obtained by Composition and Distribution Function analyzer (CODIF) instrument onboard Cluster satellite were used (*Yang et al*., 2010, 2011a, 2011b; *Zong et al*., 2012; *Ren et al*., 2016, 2017). Acceleration or deceleration of O^+ ions by the drift-bounce resonance on the dayside has been reported (*Yang et al*., 2011a; *Zong et al*., 2012). *Ren et al*. (2017) statistically analyzed the O^+ drift-bounce resonance occurrence and found that most of the events occurred on the dayside and few events in the midnight to dawn region. In addition, most of these previous studies did not determine the *m*-number from direct observations. To clarify the influence of the drift-bounce resonance on the ring current, we need to examine whether the drift-bounce resonance can occur on the nightside and accelerate or decelerate O^+ ions based on the direct measurement of the *m*-number.

In this study, we conduct an event analysis of a Pc5 wave and energetic particle flux oscillations in the nightside inner magnetosphere during the storm recovery phase on 27 March 2017, by using Exploration of energization and Radiation in Geospace “Arase”

(ERG) and Magnetospheric Multiscale 1 (MMS1) satellites data as well as ground magnetometer data. We directly estimate the *m*-number of the Pc5 wave using two methods: satellite and ground observations. Based on the estimated *m*-number, we examine if the ion flux oscillations are caused by the drift-bounce resonance. Finally, we discuss the selective acceleration of O^+ ions at the resonance energy. The following are considered to be new and significant findings of the present study: (1) we first find the drift-bounce resonance of O^+ ions in the nightside inner magnetosphere at multiple energies that predominantly contribute to the ring current, and (2) such analysis was enabled by the simultaneous observations by the recently-launched Arase and the MMS1 satellites.

2. Data Set

The Arase satellite was launched on 20 December 2016 into a highly elliptical orbit with an inclination of ~31°, an apogee of ~6 R_E, and a perigee altitude of ~460 km (*Miyoshi et al.*, 2018). Its spin period is ~8 s and the spin axis is approximately pointing to the Sun. Magnetic field data are obtained by the triaxial fluxgate magnetometer for the Magnetic Field Experiment (MGF) (*Matsuoka et al.*, 2018) onboard Arase with a sampling rate of 256 Hz. We used the spin-averaged (~8 s) data.

Medium-Energy Particle Experiments - Ion Mass Analyzer (MEP-i) instrument (*Yokota et al.*, 2017) carried by Arase can distinguish the following ion species: H^+, He^+, He^{2+}, O^+, O^{2+}, and O_2^+. MEP-i has 16 azimuthal channels, each of which has a 22.5° field of view (FOV) to cover 360° FOV. The vector normal to the plane of the azimuthal channels is perpendicular to the spin axis. One spin is divided into 16 sectors. There are 16 energy channels covering ~10 to ~180 keV/q, corresponding to the sweeping voltage (SV) of ±5 kV at a maximum. However, the SV had been set to ±3 kV during the early phase of data acquisition until 21 April 2017, and the observed energy range is 5.1–109.6 keV/q in the present event. There are three observational modes: normal (NML) mode, time-of-flight (TOF) mode, and solid-state detector (SSD) mode. We used the 2 spin-averaged (~16 s) flux data of the NML mode, which yields 16 (azimuthal sectors)×16 (spin sectors) data in one spin.

Medium-Energy Particle Experiments - Electron Analyzer (MEP-e) instrument (*Kasahara et al.*, 2018) onboard Arase detects electrons (e^-) with 16 energy channels covering 7.0–87.5 keV.

Magnetic field and electric field data are also obtained by MMS. MMS mission consists of four identical spacecraft in tetrahedral formation and spacecraft were launched in March 2015 into high inclination orbit with an apogee and a perigee of 12 and 1.2 R_E, respectively (*Burch et al.*, 2016). The fluxgate magnetometer (FGM) measures the magnetic fields

(*Russell et al*., 2016), and the electric field double probes (EDP) measures the electric fields (*Ergun et al*., 2016; *Lindqvist et al*., 2016). We surveyed the magnetic field and electric field data with a 0.125 s resolution.

Additional dataset used in this study comes from ground geomagnetic observations at Tixie (TIK, 62.35° geomagnetic latitude (GMLAT), 194.71° geomagnetic longitude (GMLON)) and Pebek (PBK, 64.31° GMLAT, 225.14° GMLON). These geomagnetic field data have a 1-s sampling rate.

3. Observations of the 27 March 2017 Event

3.1 Pc5 Wave Observations

Figures 1a and 1b show the spacecraft orbits during 1820–1910 UT on 27 March 2017 in the L-magnetic local time (MLT) plane and in the $\sqrt{X_{SM}^2+Y_{SM}^2}$ - Z_{SM} plane, where SM denotes the solar magnetic coordinates. The Arase spacecraft is located in the postmidnight region at L = 5.4–6.1 and magnetic latitude (MLAT) = −32° to −25° during the recovery phase of a geomagnetic storm with the minimum Dst of −74 nT (not shown here). MMS1 is located near Arase in MLT (Figure 1a) and gradually moving to higher latitude (Figure 1b). The separations between Arase and MMS1 in L, MLT and MLAT are $\Delta L \sim 2.0$, ΔMLT ~ 0.9 hr, and ΔMLAT ~ 9°, respectively. In this time interval, only the MMS1 satellite is located

close to Arase while the other MMS satellites are far from the Arase and MMS1 satellites. Figure 1c illustrates the footprints of Arase and MMS1 calculated with the Tsyganenko 89 model (*Tsyganenko,* 1989) at 1820–1910 UT and location of the ground stations (PBK and TIK) in geographic coordinates.

Figures 1d–1f illustrate the magnetic field observed by Arase at 1820–1910 UT in the mean field aligned (MFA) coordinates, in which 10-min moving averages are subtracted, and the radial component is perpendicular to the International Geomagnetic Reference Field (IGRF)-12 (*Thébault et al.*, 2015) model field and radially outward (B_r), and the azimuthal component (B_a) is perpendicular to both the parallel (B_p) and radial components to complete the right-handed orthogonal system. A Pc5 wave has large amplitudes in both B_r and B_a, and the peak-to-peak amplitude of B_a (~30 nT) is larger than that of B_r (~10 nT). This is the evidence of an external source and a mode coupling between poloidal and toroidal modes (e.g., *Takahashi et al*., 2018). Figure 1g illustrates the 10-s averaged B_r and E_a observed by MMS1. We find that Pc5 wave oscillations appear in both B_r and E_a, and the peak-to-peak amplitude of B_a (~12 nT, not shown) is also larger than that of B_r (~8 nT). In addition, E_a leads B_r by ~90° at 1830–1905 UT. This is the characteristic of odd mode standing oscillations in the southern hemisphere (e.g., *Dai et al*., 2013). Since the wave period of the Pc5 wave is quite long (~450 s), this Pc5 wave is likely a fundamental standing wave. Fundamental mode waves are easily detected in the off-equatorial regions,

which is consistent with both Arase and MMS1 observations that the Pc5 waves are clearly observed far from the equatorial plane.

Figure 1h shows the Y (east-west) component of the ground magnetic field at TIK and PBK from which 10-min moving averages are subtracted. These two stations are chosen because they are located close to the satellite footprints as shown in Figure 1c. A Pc5 wave with a period similar to that observed by Arase is detected at both stations. Figure 2a illustrates the power spectra of B_r observed by Arase, B_r and E_a observed by MMS1, and Y component of the magnetic field at TIK and PBK during 1830–1910 UT. We find spectral peaks at 2–2.5 mHz in all power spectra, which indicates that the Pc5 waves observed by Arase, MMS1, and the ground magnetometers at TIK and PBK are identical.

3.2 Particle Flux Oscillations Observed by MEP

We investigate the particle fluxes measured by MEP-i and MEP-e. Figures 1i–1k are the 60-s averaged omni-directional residual fluxes ($(J-J_0)/J_0$), where J is the particle flux and J_0 is the 10-min moving average, of H^+ and O^+ ions, and of electrons. Figure 1i shows that H^+ fluxes in wide energy ranges oscillate with the Pc5 wave period, and their oscillation amplitudes are large at $\geq$ 56.3 keV during 1830–1910 UT. Figure 1j shows that the O^+ ion fluxes are also clearly modulated at 1830–1910 UT with the same period of the Pc5 wave. The oscillation amplitudes are larger at $\geq$ 56.3 keV and $\leq$ 18.6 keV. We can find negative

energy dispersions (e.g., *Southwood et al*., 1981) for both H^+ at ≥ 56.3 keV and O^+ ion fluxes at ≥ 56.3 keV and ≤ 18.6 keV in Figures 1i and 1j. Despite the large electron flux oscillations at 14.3–35.0 keV, the energy dispersion signature cannot be seen in Figure 1k. We calculate the omni-directional flux ratio of O^+/H^+ (Figure 1l), which exhibit a distinct structure in the O^+/H^+ flux ratio. The ratio is ~0.1 until 1825 UT, and then it reaches the maximum of ~0.4 at ≤ 23.3 keV and ≥ 45.1 keV during 1840–1910 UT, corresponding to the O^+ ion flux oscillations.

Figures 2b and 2c illustrate the power spectra of the residual fluxes ($(J-J_0)/J_0$) of H^+ and O^+ ions at different energies. Clear spectral peaks can be seen in wide energy ranges for both H^+ and O^+ ions at 2–2.5 mHz, which is similar to the Pc5 wave frequency. The spectral peaks of O^+ ions are larger than those of H^+. In Figures 2d and 2e, we plot power spectral peaks for H^+ and O^+ ions near 2–2.5 mHz for different energies. The peak power of H^+ at ≥ 56.3 keV is more than ~3 times larger than that at lower energies. It also should be noted that we can find a small peak at ~7 keV (Figure 2d), though the width of the peak is too narrow without plateau structure like that at high energy, indicating that the H^+ flux oscillations mainly occur at higher energies. Figure 2e shows two energy bands with large peak power for O^+ ions at ≥ 56.3 keV and ≤ 18.6 keV, while there is a "dip" of the peak power of O^+ ions at 23.3–45.1 keV. This structure of the peak power is similar to that of O^+/H^+ in Figure 1l, suggesting a relation between O^+ ion oscillations and the O^+/H^+

structure. The power enhancement of H^+ and O^+ ions may extend up to ≥ 109.6 keV, which cannot be detected with the MEP-i.

4. Discussion

The value of the *m*-number generally reflects the energy source of Pc5 waves: external solar wind for a small *m*-number or internal plasma instability for a large *m*-number. Also, the drift-bounce resonance mode and the resonance energy strongly depend on the *m*-number. In this section, we estimate the value of the *m*-number, and discuss the energy source and the resonance characteristics.

4.1 Estimation of *m*-number of the Pc5 Wave

The Pc5 wave is observed by Arase, MMS1, and ground stations at TIK and PBK. We examine the *m*-number by two methods.

First, we estimate the *m*-number using Arase and MMS1 data. Figure 1a shows that both satellites are close each other in MLT, but not close in *L*. To calculate the *m*-number, we assume that the wave structure is uniform in *L*. We can estimate the *m*-number from a phase delay of the Pc5 waves observed by two satellites that are azimuthally separated; that is, $m = \Delta\theta/\Delta\varphi$, where $\Delta\theta$ is the phase difference, and $\Delta\varphi$ is the azimuthal separation between

satellites. Figures 1d and 1g show a clear time lag in B_r. We determine a time lag that provides the maximum value of the cross-correlation coefficient between B_r observed by Arase and MMS1. Cross-correlation analysis shows that the time delay is 240 s at 1830–1910 UT. Since Figure 2a shows the wave period of ~ 450 s, we obtain $\Delta\theta \sim -192°$, where the negative sign means westward propagation. $\Delta\varphi$ between Arase and MMS1 is ~13° at 1830–1910 UT. Thus, these values of $\Delta\varphi$ and $\Delta\theta$ give $m \sim -15$.

Second, we estimate the m-number using ground magnetometer data at TIK and PBK with the same method as first estimation. The cross-correlation analysis at 1830–1910 UT gives 305 s time delay between TIK and PBK, which corresponds to $\Delta\theta \sim -244°$, and $\Delta\varphi = 30.4°$ in the geomagnetic coordinate. Then, m-number is estimated to be $m \sim -8$.

From the two independent methods, we obtain the similar values of $m \sim -8$ to -15. (Although there is a possibility that the phase difference includes a $2n\pi$ ambiguity, the cross-correlation coefficients become maximum when $n = 0$.) These values are consistent with the fact that the Pc5 wave is observed on the ground with a less ionospheric screening effect. According to *Hughes et al*. (1976), the wave amplitude of $|m| = 10$ on the ground is ~86% that of $m = 0$. The westward propagation in the morning sector is also consistent with the result of previous studies (e.g., *Baker et al*., 2003).

4.2 Energy Source of the Pc5 Wave

Pc5 waves are mainly excited on the dayside magnetosphere by the Kelvin-Helmholtz (K-H) instability due to high solar wind velocity, solar wind dynamic pressure variation, and ion foreshock (e.g., *Ukhorskiy et al*., 2009; *Takahashi et al*., 2016). Past studies on ULF wave distributions showed that Pc5 waves can occur in the dawn to the postmidnight region (e.g., *Anderson et al*., 1990; *Nosé et al*., 1995; *Liu et al*., 2009). The Pc5 wave in the present study has quite large amplitude in the azimuthal component of the magnetic field on the nightside (Figure 1e) when the solar wind velocity is high (~600–650 km/s) according to the OMNI database. Pc5 waves excited by solar wind tend to have small *m*-number, which is consistent with the above result ($m \sim -8$ to -15). Thus, we suggest that this Pc5 wave is excited by solar wind, not by internal plasma instabilities.

4.3 Examination of the Flux Oscillations

Flux oscillations associated with ULF waves are often observed in the magnetosphere. Betatron acceleration, drift-bounce resonant interaction, and radial convection of particles are proposed as the reason of the flux oscillations (e.g., *Southwood et al*., 1981; *Takahashi et al*., 1985; *Korotova et al*., 2015). Direct measurements of the *m*-number from the satellite and ground observations enable us to calculate the resonance energy based on equation (1). The approximation of ω_b and ω_d in a dipole magnetic field are given by $\omega_b = \frac{\pi\sqrt{2W/m_i}}{2LR_E T(\sin\alpha_E)}$ and $\omega_d = -\frac{6WLP(\sin\alpha_E)}{qB_E{R_E}^2} + \frac{2\psi_0 L^3 \sin\varphi}{B_E{R_E}^2} + \Omega_E$, where m_i is the ion mass, R_E is the Earth's radius,

α_E is the pitch angle at the geomagnetic equator, B_E is the equatorial magnetic field at the surface of the Earth, q is the electric charge, φ is the azimuthal angle which is positive eastward with 0° at midnight, Ω_E is the angular frequency of the corotation of the Earth, and ψ_0 is the electric potential of the convection electric field. We adopt B_E = 30,000 nT, and the following formulae: $T(\sin\alpha_E) = 1.351 - 0.925\sin\alpha_E + 0.558\sin^2\alpha_E - 0.248\sin^3\alpha_E$ and $P(\sin\alpha_E) = 0.340 + 0.226\sin\alpha_E - 0.154\sin^2\alpha_E + 0.088\sin^3\alpha_E$ (*Hamlin et al*., 1961; *Yang et al*., 2011a; *Oimatsu et al*., 2018). We use the Volland-Stern model electric potential as ψ_0 (*Volland*, 1973; *Stern*, 1975; *Maynard and Chen*, 1975). Figure 3 shows the theoretical drift-bounce resonance energy with fundamental mode wave (N = 0 and 2) as a function of the m-number in a dipole magnetic field for H^+ and O^+ ions. Particles with equatorial pitch angle of 90° most effectively resonate with fundamental mode waves. In general, ULF waves are not monochromatic, and wave frequency and m-number have a finite bandwidth (e.g., *Takahashi et al*., 1990; *Korotoba et al*., 2015). We use wave frequencies of 1.75 and 3 mHz, L = 5.8, and a local pitch angle of 90° to calculate the resonance energy. The vertical dashed lines denote m = −8 and −15, which are estimated from the satellite and ground observations. There are two solutions: $\omega \sim m\omega_d$ (N = 0, drift resonance) and $\omega \sim 2\omega_b$ (N = 2, bounce resonance). For the finite bandwidths of m-number and wave frequency, the drift resonance energy of H^+ and O^+ ions are estimated to be ~70–200 keV for both ion species, and the bounce resonance energies are estimated to be ~0.2–0.6 keV for H^+ and

~3–9 keV for O^+ ions, respectively. These results of the theoretical resonance energy are generally consistent with the observational facts of large power spectral peaks for both H^+ and O^+ ions at ≥ 56.3 keV (drift resonance) and for O^+ ions at ≤ 18.6 keV (bounce resonance) in Figures 2d and 2e.

Drift-bounce resonance theory predicts a 180° phase shift over the resonance energy (e.g., *Southwood et al*., 1981; *Takahashi et al*., 1990). Figures 1i–1j show the dispersive flux peaks for H^+ at ≥ 56.3 keV and for O^+ ions at ≥ 56.3 keV and ≤ 18.6 keV, which are similar to the past observational results (e.g., *Ren et al*., 2016). This implies the drift-bounce resonance for H^+ and O^+ ions because of the measurable phase shifts over the energy channels. In this study, the drift resonance and bounce resonance for O^+ ions are simultaneously observed for the first time. Previous studies found O^+ drift-bounce resonance at ≤ 40 keV because of the instrument limitation of the energy coverage. The wide energy coverage of MEP-i enables us to find the resonances at multiple energies. The phase shift of O^+ ion flux at ≤ 18.6 keV is much larger than those of H^+ and O^+ ion fluxes at ≥ 56.3 keV (Figures 1i and 1j). We suppose that the drift resonance energy, which is estimated to be 70–200 keV from the theoretical calculations, is close to or higher than the upper limit of the energy coverage of MEP-i (109.6 keV) and, consequently, the overall phase shifts cannot be detected. Electron fluxes at 14.3–35.0 keV oscillate, but they do not

show energy dispersion (Figure 1k), indicating that the electron flux oscillations are not caused by the drift-bounce resonance.

The observed Pc5 wave has a toroidal mode component. If there is a gradient of particle flux distribution in the azimuthal direction, toroidal mode waves can influence the particle fluxes. However, the variation of the particle distribution in the azimuthal direction is expected to be smaller than that in the radial direction. Therefore, the particle fluctuations are mainly generated by poloidal mode waves.

4.4 Implication of Selective Acceleration of O^+ Ions

O^+/H^+ flux ratio becomes high at two energy bands ($\leq$ 23.3 keV and $\geq$ 45.1 keV) corresponding to the energy ranges of the drift resonance and the bounce resonance of ions during 1830–1910 UT in Figure 1l. One may think that this is caused by the spatial effect. However, in such case, the O^+/H^+ ratio is expected to become high in wider energy ranges, unlike what shown by the present results. Hence, we suggest that the enhancement of O^+/H^+ flux ratio in the low-energy band ($\leq$ 23.3 keV) is mainly caused by selective acceleration of O^+ ions due to the bounce resonance at $\leq$ 18.6 keV, because only the bounce resonance of O^+ ions occurs without that of H^+ ions at the same energy. It would be appropriate to consider that the solar wind generates the Pc5 wave and it feeds energy to the O^+ ions through the bounce resonance. *Mitani et al*. (2018) proposed that the drift-bounce

resonance contributes to the selective penetration of O^+ ions into the inner magnetosphere from the plasma sheet during the late main phase to early recovery phase, which is consistent with our scenario. The present study first demonstrates the selective acceleration of O^+ ions due to the bounce resonance in the nightside inner magnetosphere. The enhancement of the O^+/H^+ flux ratio in the high-energy band ($\geq$ 45.1 keV) may be due to the acceleration efficiency of the drift resonance between H^+ and O^+ ions ($\geq$ 56.3 keV). It should be examined in the future how effectively the drift resonance take place for H^+ and O^+ ions, which is expected to depend on the radial and energy gradients of the phase space density of ion species (e.g., *Southwood et al*., 1969).

5. Conclusions

We first examine the drift-bounce resonance between a fundamental mode Pc5 pulsation and O^+ ions in the nightside inner magnetosphere at L = 5.4–6.1 during a storm recovery phase on 27 March 2017, using data from Arase, MMS1, and ground magnetometers at TIK and PBK. We directly estimate the m-number of the Pc5 wave to be $m \sim -8$ to -15 by two independent methods using satellites and ground observations. The H^+ fluxes show the largest oscillation amplitude at $\geq$ 56.3 keV and the O^+ ion fluxes also show the largest amplitude at the same energy ($\geq$ 56.3 keV) and at $\leq$ 18.6 keV. The O^+/H^+ flux ratio

becomes higher during the ion flux oscillations at ≤ 23.3 keV and ≥ 45.1 keV. The theoretical drift resonance energy is ~70–200 keV for both H^+ and O^+ ions, while the theoretical bounce resonance energy is ~3–9 keV for O^+ ions. These theoretical resonance energies are consistent with the results of the Arase/MEP-i observation. The H^+ and O^+ ion oscillations at ≥ 56.3 keV are generated through the drift resonance, while the O^+ ion oscillations at ≤ 18.6 keV are caused by the bounce resonance. These resonances of O^+ ions at multiple energies are simultaneously observed for the first time. The enhancement of the O^+/H^+ flux ratio at ≤ 18.6 keV indicates a selective acceleration of O^+ ions due to the bounce resonance.

Acknowledgments

We thank Dr. K. Takahashi for his valuable comments. We appreciate all people dedicated to the Arase mission. The works of MT and YM were partly done at ERG-SC. Science data of the Arase satellite were obtained from the ERG Science Center operated by ISAS/JAXA and ISEE/Nagoya University (http://ergsc.isee.nagoya-u.ac.jp/index.shtml.en). The Arase satellite data will be publicly available via ERG Science Center on a project-agreed schedule. The present study analyzed the MGF L2 v01.01 data, the MEP-i L2 v01_00 data, and the MEP-e L2 v01_00 data. The magnetic field and electric field data observed by FGM and EDP onboard MMS1 are available via MMS science data center at https://lasp.colorado.edu/mms/sdc/public/. Solar wind data were obtained from OMNI database at https://omniweb.gsfc.nasa.gov. The Dst index was provided by the World Data Center for Geomagnetism, Kyoto, and is available at http://wdc.kugi.kyoto-u.ac.jp. This study is supported by Japan Society for the Promotion of Science (JSPS), Grant-in-Aid for Scientific Research (B) (grant 16H04057), Challenging Research (Pioneering) (17K18804), and Grant-in-Aid for Specially Promoted Research (16H06286). YM is supported by Japan Society for the Promotion of Science (JSPS), Grant-in-Aid for Scientific Research on Innovative Areas (grant 15H05815).

References

Anderson, B. J., M. J. Engebretson, S. P. Rounds, L. J. Zanetti, and T. A. Potemra (1990), A statistical study of Pc 3–5 pulsations observed by the AMPTE/CCE Magnetic Fields Experiment, 1. Occurrence distributions, J. Geophys. Res., 95(A7), 10495–10523, doi:10.1029/JA095iA07p10495.

Baker, G., E. F. Donovan, and B. J. Jackel, A comprehensive survey of auroral latitude Pc5 pulsation characteristics, J. Geophys. Res., 108(A10), 1384, doi:10.1029/2002JA009801, 2003.

Burch, J.L., Moore, T.E., Torbert, R.B. et al. (2016), Magnetospheric Multiscale Overview and Science Objectives, Space Sci Rev, 199: 5, doi:10.1007/s11214-015-0164-9.

Dai, L., et al. (2013), Excitation of poloidal standing Alfvén waves through drift resonance wave-particle interaction, Geophys. Res. Lett., 40, 4127-4132, doi:10.1002/grl.50800.

Dai, L., et al. (2015), Storm time occurrence and spatial distribution of Pc4 poloidal ULF waves in the inner magnetosphere: A Van Allen Probes statistical study, J. Geophys. Res. Space Physics, 120, 4748–4762, doi:10.1002/2015JA021134.

Elkington, S. R., M. K. Hudson, and A. A. Chan (2003), Resonant acceleration and diffusion of outer zone electrons in an asymmetric geomagnetic field, J. Geophys. Res., 108(A3), 1116, doi: 10.1029/2001JA009202.

Ergun, R.E., Tucker, S., Westfall, J. et al. (2016), The Axial Double Probe and Fields Signal

Processing for the MMS Mission, Space Sci Rev, 199: 167. doi:10.1007/s11214-014-0115-x.

Hamlin, D. A., R. Karplus, R. C. Vik, and K. M. Watson (1961), Mirror and azimuthal drift frequencies for geomagnetically trapped particles, J. Geophys. Res., 66(1), 1–4, doi:10.1029/JZ066i001p00001.

Hughes, W. J., and D. J. Southwood (1976), The screening of micropulsation signals by the atmosphere and ionosphere, J. Geophys. Res., 81, 3234, doi:10.1029/JA081i019p03234.

Kasahara, S., S. Yokota, T. Mitani, K. Asamura, M. Hirahara, Y. Shibano, and T. Takashima (2018), Medium-energy particle experiments electron analyzer (MEP-e) for the exploration of energization and radiation in geospace (ERG) mission, Earth, Planets and Space, 70:69, doi: 10.1186/s40623-018-0847-z.

Keika, K., L. M. Kistler, and P. C. Brandt (2013), Energization of O^+ ions in the Earth's inner magnetosphere and the effects on ring current buildup: A review of previous observations and possible mechanisms, J. Geophys. Res. Space Physics, 118, 4441–444, doi:10.1002/jgra.50371.

Korotova, G. I., D. G. Sibeck, K. Tahakashi, L. Dai, H. E. Spence, C. A. Kletzing, J. R. Wygant, J. W. Manweiler, P. S. Moya, K. J. Hwang, and R. J. Redmon (2015), Van Allen Probe observations of drift-bounce resonances with Pc 4 pulsations and wave-particle interactions in the pre-midnight inner magnetosphere, Ann. Geophys., 33 (8), 955–964,

doi:10.5194/angeo-33-955-2015.

Le, G., et al. (2017), Global observations of magnetospheric high-m poloidal waves during the 22 June 2015 magnetic storm, Geophys. Res. Lett., 44, 3456–3464, doi:10.1002/2017GL073048.

Li, X., M. Hudson, A. Chan, and I. Roth (1993), Loss of ring current O^+ ions due to interaction with Pc 5 waves, J. Geophys. Res., 98(A1), 215-231, doi:10.1029/92JA01540.

Lindqvist, P. A., Olsson, G., Torbert, R. B., King, B., Granoff, M., Rau, D., ... & Macri, J. (2016). The spin-plane double probe electric field instrument for MMS. Space Science Reviews, 199(1-4), 137-165.

Liu, W., T. E. Sarris, X. Li, S. R. Elkington, R. Ergun, V. Angelopoulos, J. Bonnell, and K. H. Glassmeier (2009), Electric and magnetic field observations of Pc4 and Pc5 pulsations in the inner magnetosphere: A statistical study, J. Geophys. Res., 114, A12206, doi:10.1029/2009JA014243.

Matsuoka et al. (2018), The ARASE (ERG) magnetic field investigation, Earth, Planets and Space, 70:43, doi:10.1186/s40623-018-0800-1.

Maynard, N. C., and A. J. Chen (1975), Isolated cold plasma regions: Observations and their relation to possible production mechanisms, J. Geophys. Res., 80(7), 1009–1013, doi:10.1029/JA080i007p01009.

Min, K., K. Takahashi, A. Y. Ukhorskiy, J. W. Manweiler, H. E. Spence, H. J. Singer, S. G.

Claudepierre, B. A. Larsen, A. R. Soto-Chavez, and R. J. Cohen (2017), Second harmonic poloidal waves observed by Van Allen Probes in the dusk-midnight sector, J. Geophys. Res. Space Physics, 122, doi:10.1002/2016JA023770.

Mitani, K., Seki, K., Keika, K., Gkioulidou, M., Lanzerotti, L. J., Mitchell, D. G., & Kletzing, C. A. (2018). Radial transport of higher-energy oxygen ions into the deep inner magnetosphere observed by Van Allen Probes. Geophysical Research Letters, 45. doi: 10.1029/2018GL077500.

Miyoshi, Y., I. Shinohara, T. Takashima, K. Asamura, N. Higashio, T. Mitani, S. Kasahara, S. Yokota, Y. Kazama, S-Y. Wang, S.W. Tam, P. Ho, Y. Kasahara, Y. Kasaba, S. Yagitani, A. Matasuoka, H. Kojima, Y. Katoh, K. Shiokawa, K. Seki (2018), Geospace Exploration Project ERG, Earth, Planets and Space, doi: 10.1186/s40623-018-0862-0.

Nosé, M., Iyemori, T., Sugiura, M., & Slavin, J. A. (1995). A strong dawn/dusk asymmetry in Pc5 pulsation occurrence observed by the DE-1 satellite. Geophysical research letters, 22(15), 2053-2056.

Oimatsu, S., M. Nosé, K. Takahashi, K. Yamamoto, K. Keika, C. A. Kletzing, C. W. Smith, R. J. MacDowall, D. G. Mitchell (2018), Van Allen Probes observations of drift-bounce resonance and energy transfer between energetic ring current protons and poloidal Pc4 wave, J. Geophys. Res. Space Physics, 123, doi: 10.1029/2017JA025087.

Ren, J., Q.-G. Zong, X.-Z. Zhou, R. Rankin, and Y.-F. Wang (2016), Interaction of ULF

waves with different ion species: Pitch angle and phase space density implications, J. Geophys. Res. Space Physics, 121, 9459–9472, doi:10.1002/2016JA022995.

Ren, J., Q. G. Zong, X. Z. Zhou, R. Rankin, Y. F. Wang, S. J. Gu, and Y. F. Zhu (2017), Phase relationship between ULF waves and drift-bounce resonant ions: A statistical study, J. Geophys. Res. Space Physics, 122, 7087–7096, doi:10.1002/2016JA023848.

Russell, C.T., Anderson, B.J., Baumjohann, W. et al. (2016), The Magnetospheric Multiscale Magnetometers, Space Sci Rev, 199: 189. doi:10.1007/s11214-014-0057-3.

Southwood, D. J., Dungey, J. W., Etherington, R. J. (1969). Bounce resonant interaction between pulsations and trapped particles, Planetary and Space Science, 17(3), 349-361, doi:10.1016/0032-0633(69)90068-3.

Southwood, D. J., and M. G. Kivelson (1981), Charged particle behavior in low-frequency geomagnetic pulsations 1. Transverse waves, J. Geophys. Res., 86(A7), 5643-5655, doi:10.1029/JA086iA07p05643.

Southwood, D. J., and M. G. Kivelson (1982), Charged particle behavior in low-frequency geomagnetic pulsations, 2. Graphical approach, J. Geophys. Res., 87(A3), 1707-1710, doi:10.1029/JA087iA03p01707.

Stern, D. P. (1975), The motion of a proton in the equatorial magnetosphere, J. Geophys. Res., 80(4), 595–599, doi:10.1029/JA080i004p00595.

Takahashi, K., P. R. Higbie, and D. N. Baker (1985), Azimuthal propagation and frequency

characteristic of compressional Pc 5 waves observed at geostationary orbit, J. Geophys. Res., 90(A2), 1473–1485, doi:10.1029/JA090iA02p01473.

Takahashi, K., R. W. McEntire, A. T. Y. Lui, and T. A. Potemra (1990), Ion flux oscillations associated with a radially polarized transverse Pc 5 magnetic pulsation, J. Geophys. Res., 95, 3717–3731, doi:10.1029/JA095iA04p03717.

Takahashi, K., M. D. Hartinger, D. M. Malaspina, C. W. Smith, K. Koga, H. J. Singer, D. Fru□hauff, D. G. Baishev, A. V. Moiseev, and A. Yoshikawa (2016), Propagation of ULF waves from the upstream region to the midnight sector of the inner magnetosphere, J. Geophys. Res. Space Physics, 121, 8428–8447, doi:10.1002/2016JA022958.

Takahashi, K., Oimatsu, S., Nosé, M., Min, K., Claudepierre, S. G., **Chan, A., ... Kin**

(2018). **Van Allen Probes observations of second** Van Allen probes observations of second waves. Journal of Geophysical Research: Space Physics, 123. https://doi.org/10.1002/2017JA024869.

Thébault, E., Finlay, C. C., Beggan, C. D., Alken, P., Aubert, J., Barrois, O., et al. (2015). International Geomagnetic Reference Field: The 12th generation. Earth, Planets and Space, 67(1), 79. https://doi.org/10.1186/s40623-015-0228-9.

Tsyganenko, N. A. (1989), A magnetospheric magnetic field model with a warped tail current sheet, Planet. Space Sci., 37, 5–20, doi: 10.1016/0032-0633(89)90066-4.

Ukhorskiy, A. Y., Sitnov, M. I., Takahashi, K., and Anderson, B. J.: Radial transport of

radiation belt electrons due to stormtime Pc5 waves, Ann. Geophys., 27, 2173-2181, https://doi.org/10.5194/angeo-27-2173-2009, 2009.

Yang, B., Q.-G. Zong, Y. F. Wang, S. Y. Fu, P. Song, H. S. Fu, A. Korth, T. Tian, and H. Reme (2010), Cluster observations of simultaneous resonant interactions of ULF waves with energetic electrons and thermal ion species in the inner magnetosphere, J. Geophys. Res., 115, A02214, doi:10.1029/2009JA014542.

Yang, B., Q. G. Zong, S. Y. Fu, X. Li, A. Korth, H. S. Fu, C. Yue, and H. Reme (2011a), The role of ULF waves interacting with oxygen ions at the outer ring current during storm times, J. Geophys. Res., 116, A01203, doi:10.1029/2010JA015683.

Yang, B., et al. (2011b), Pitch angle evolutions of oxygen ions driven by storm time ULF poloidal standing waves, J. Geophys. Res., 116, doi:A03207, doi:10.1029/2010JA016047.

Yokota et al. (2017), Medium-energy particle experiments–ion mass analyzer (MEP-i) onboard ERG (Arase), Earth, Planets and Space, 69:172, doi:10.1186/s40623-017-0754-8.

Volland, H. (1973), A semiempirical model of large-scale magnetospheric electric fields, J. Geophys. Res., 78(1), 171-180, doi:10.1029/JA078i001p00171.

Zong, Q.-G., Y. F. Wang, H. Zhang, S. Y. Fu, H. Zhang, C. R. Wang, C. J. Yuan, and I. Vogiatzis (2012), Fast acceleration of inner magnetospheric hydrogen and oxygen ions by shock induced ULF waves, J. Geophys. Res., 117, A11206, doi:10.1029/2012JA018024.

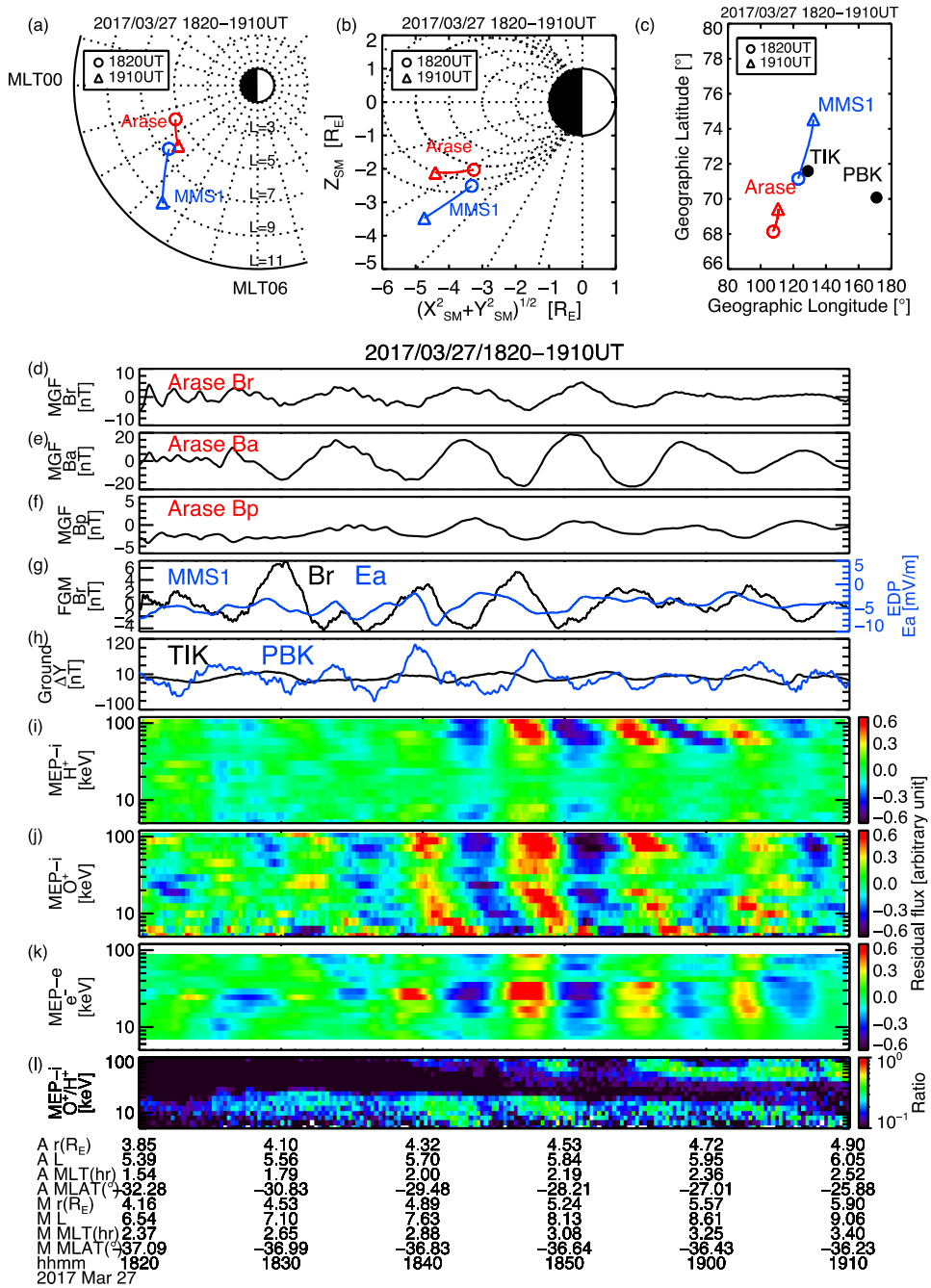

Figure 1.

Satellite orbits, satellite data, and ground station data for 1820–1910 UT on 27 March 2017. First letters “A” and “M” of orbit information denote “Arase” and “MMS1”, respectively. (a) Arase and MMS1 satellite orbits in the *L*-MLT plane. (b) Arase and MMS1 orbits in the $\sqrt{X_{SM}^2+Y_{SM}^2}$ - Z_{SM} plane of SM coordinates. (c) Satellite footprints and the location of the ground magnetic stations at Tixie (TIK) and Pebek (PBK) in geographic coordinates. (d, e, f) Magnetic fields in radial (B_r), azimuthal (B_a), and parallel components (B_p) observed by MGF. (g) Magnetic field in the radial component (black) and electric field in the azimuthal component (E_a, blue) observed by MMS1. (h) Ground magnetic field in the Y (east-west) component at TIK (black) and PBK (blue). (i, j, k) 60-s averaged residual fluxes of H^+ and O^+ ions detected by MEP-i, and 60-s averaged residual flux of electrons detected by MEP-e. (l) O^+/ H^+ ratio of the omni-directional fluxes.

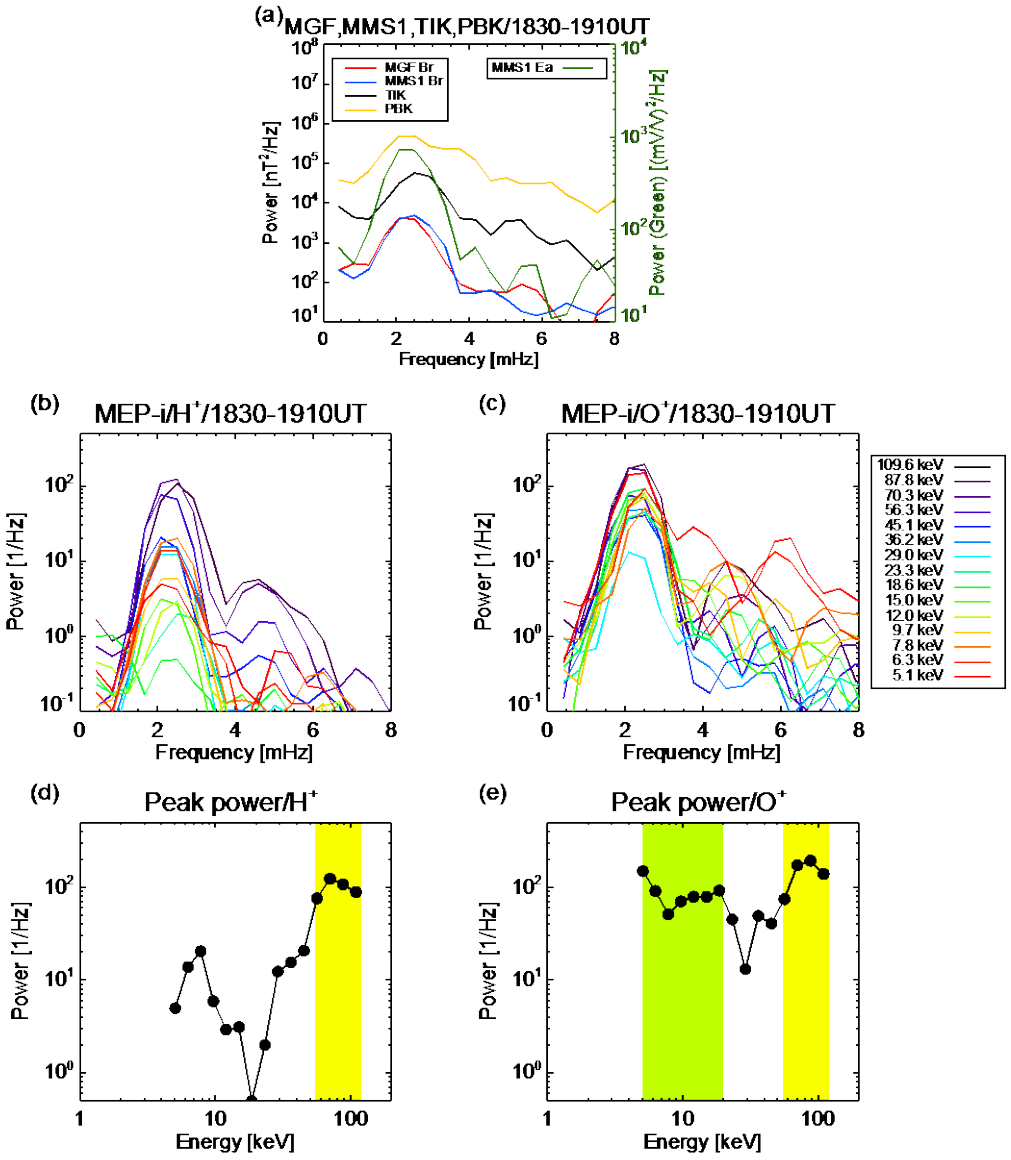

Figure 2.

(a) Power spectra of the magnetic field in the radial component observed by MGF and MMS1, the magnetic field in the Y component observed at TIK and PBK, and the electric field in the azimuthal component observed by MMS1 at 1830–1910 UT. (b, c) Power spectra of the residual fluxes of H^+ and O^+ ions detected by MEP-i at 1830–1910 UT. Colors delineate different energies as indicated in the legend. (d, e) Spectral peak power of H^+ and O^+ ion fluxes at ~2–3 mHz as a function of energies.

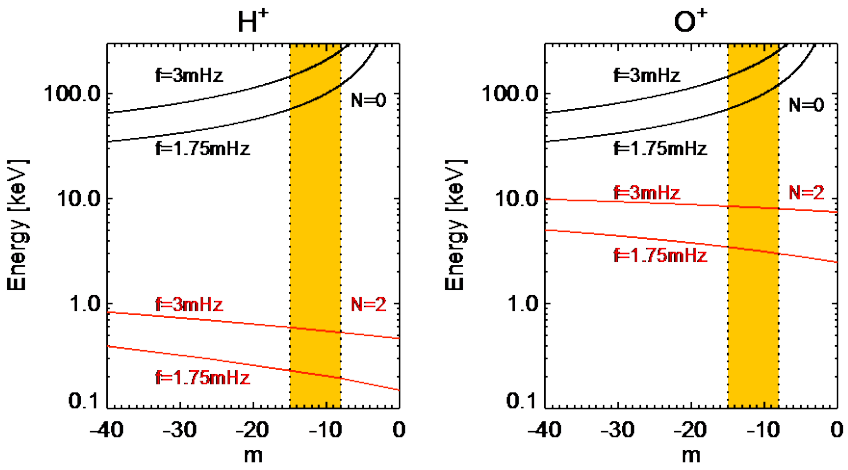

Figure 3.

Resonance energies of H^+ and O^+ ions with fundamental mode (N = 0, 2) waves as a function of m, when a dipole magnetic field is assumed. We use frequencies of 1.75 and 3 mHz, L = 5.8, and a local pitch angle of 90° to calculate the energy.